Carbon 129 (2018) 335–341

Contents lists available at ScienceDirect

Carbon

journal homepage: www.elsevier.com/locate/carbon

Template-free synthesis of coral-like nitrogen-doped carbon dots/Ni_3S_2/Ni foam composites as highly efficient electrodes for water splitting

Yuan Rao [a, b, 1], Hui Ning [a, 1], Xiao Ma [a], Yang Liu [a], Yang Wang [a], Hui Liu [a], Jialiang Liu [a], Qingshan Zhao [a], Mingbo Wu [a, *]

[a] State Key Laboratory of Heavy Oil Processing, College of Chemical Engineering, China University of Petroleum (East China), Qingdao, 266580, China
[b] Institute of Fundamental and Frontier Sciences, University of Electronic Science and Technology of China, Chengdu, 610054, China

ARTICLE INFO

Article history:
Received 26 September 2017
Received in revised form
21 November 2017
Accepted 10 December 2017
Available online 11 December 2017

ABSTRACT

Non-noble, high-efficient electrodes with excellent durability are desirable for water splitting. Herein, a facile strategy has been proposed to in-situ grow nitrogen-doped carbon dots (NCDs) decorated Ni_3S_2 on Ni foam (NCDs/Ni_3S_2/NF) by hydrothermal treatment of Ni foam in water solution of thiourea and NCDs. Interestingly, coral-like NCDs/Ni_3S_2/NF composites are unprecedentedly prepared without any templates, where the Ni_3S_2 nanorods mainly expose {021} high-index facets. The resultant NCDs/Ni_3S_2/NF composites are directly used as self-supported electrodes for overall water splitting which deliver a current density of 10 mA cm^{-2} at 1.50 V with excellent durability in 1.0 M KOH solution.

1. Introduction

Hydrogen has been considered as an alternative clean energy for fossil fuels, and electrochemical water splitting is a well-established technology for producing hydrogen to store and transport peak excess electricity from intermittent renewable energy resources (such as wave power, wind and solar energy) [1]. However, the water electrolysis usually requires high over-potentials for both oxygen evolution reaction (OER) and hydrogen evolution reaction (HER) to deliver considerable reaction rates. To be specific, around 50% (1.8–2 V instead of 1.23 V) excess potential is required in an industrial electrolyzer, which limits the possibility of massive hydrogen production in a cost-effective manner [2]. Therefore, more active electrocatalysts for OER and HER are desired. At present, Ir/Ru-based oxides [3] and Pt-group materials [4] are normally used as the benchmark electrocatalysts for OER and HER, respectively. Nevertheless, their scarcity and high cost restrict their application on a global scale. Therefore, tremendous efforts have been devoted to design and synthesize highly efficient OER and HER catalysts from earth-abundant elements [5–12]. Ni_3S_2, a low-cost metal chalcogenide that exists in nature, shows high conductivity and intrinsic metallic behavior rendering it potential candidate for overall water splitting [13]. However, most of the Ni_3S_2-based materials give unsatisfied electrocatalytic performances toward OER and/or HER, and poor durability during long-term operation [14–16]. In recent years, Carbon dots (CDs) have demonstrated great potential application as electro-/photocatalysts due to their ultrafine sizes (<10 nm) and environmentally friendly features [17–19]. By heteroatom doping, the application of CDs has been further expanded [20]. Especially, the nitrogen-doped CDs (NCDs) can form composites with metal compounds to enhance its intrinsic electrocatalytic performance [21].

Herein, a template-free strategy has been proposed to in-situ grow NCDs/Ni_3S_2 nano arrays on the surface of Ni foam as a self-supported electrode for water splitting. The hierarchal structure and decorated NCDs enhance the activity and durability of Ni_3S_2 in electrocatalytic water splitting.

2. Experimental

2.1. Chemicals and reagents

Ni foam (NF) was purchased from Suzhou Jia Shi De Foam Metal Co. Ltd. Pt/C (20 wt%), Nafion (5 wt%) and RuO_2 were purchased from Sigma-Aldrich Chemical Reagent Co. Ltd. Thiourea,

* Corresponding author.
E-mail address: wumb@upc.edu.cn (M. Wu).
[1] These authors contributed equally to this work.

https://doi.org/10.1016/j.carbon.2017.12.040
0008-6223/

ammonium hydroxide (25–28 wt%) and dichloromethane were purchased from Sinopharm Chemical Reagent Co. Ltd. Petroleum coke calcinated at 1500 °C and the oil source of petroleum pitch were from China National Offshore Oil Corporation. Highly purified water (18.2 MΩ at 25 °C) was provided by a Millipore system.

2.2. Synthesis of NCDs

The proposed method to prepare NCDs is shown in Fig. 1a. Petroleum coke (10.0 g) was added into the mixture of 30 mL dichloromethane and 1.0 g petroleum pitch (as a binder) to form a paste. After evaporating most dichloromethane, the as-prepared paste was moulded into a discoid precursor by hot-compaction treatment. A disk electrode with the diameter of ~28 mm (~2.7 g) was obtained after calcinating in a tube furnace under N_2 at 800 °C for 2 h. Then two petroleum coke-based electrodes as made were inserted into 150 mL 5 wt% ammonia solution as the working electrode and the counter electrode. Static potential of 30 V was applied to the system using a direct current (DC) power. After 4 h electrochemical oxidation, the anode disk electrode corroded completely, the mixture was filtered by a filter membrane (0.22 μm) to remove the larger fractions. Then the alkalescence solution was neutralized through evaporating the excess ammonia under 40 °C to obtained dark-yellow NCDs solution. Finally, the NCDs powders can be collected through freeze drying.

2.3. Synthesis of NCDs/Ni_3S_2/NF and Ni_3S_2/NF

The proposed method to synthesis NCDs/Ni_3S_2/NF composites is shown in Fig. 2. To remove the nickel oxides layer on the surface of NF, the purchased NF (1 cm × 4 cm) was sonicated in acetone and 3 M HCl solution for 20 min in sequence, rinsed with water and ethanol separately, then dried by an electric blower. The cleaned NF was immersed into a 60 mL Teflon-lined stainless steel autoclave filled with a homogeneous mixture of 3 mmol thiourea (0.228 g) and 30 mL 1.0 mg/mL NCDs solution, which was sealed and placed in a rotating oven at 160 °C for 4 h. The resultant material was rinsed with ethanol and dried at 60 °C for 1 h. For comparison, Ni_3S_2/NF was synthesized in a mixture of 3 mmol thiourea (0.228 g) and 30 mL deionized water under the same operating conditions. The weight increment (x mg) of NF ascribes to the growth of Ni_3S_2 and the combination of NCDs. To evaluate the loading mass more precisely, the weight increment (y mg) of Ni_3S_2/NF can be firstly weighted, Ni_3S_2 loading = y mg × ($M_{Ni3S2}/2M_S$) = y mg × (240/64) = 3.75y mg, NCDs loading = (x - y) mg, the total loading mass = 3.75y mg + (x − y) mg = (x + 2.75y) mg, where M is the molecular weight or atomic weight. For NCDs/Ni_3S_2/NF electrode, the loading mass of Ni_3S_2 is about 3.7 mg cm^{-2}, the loading mass of NCDs is about 0.5 mg cm^{-2}, thus the total loading mass is about 4.2 mg cm^{-2}. All the calculated values represent the average results of five samples.

2.4. Materials characterizations

The XRD patterns of resultant materials were acquired on a PANalytical X-ray Diffractometer with Cu Kα radiation (λ = 1.5418 Å). The Raman spectra were recorded by a Renishaw Raman system model 2000 spectrometer. UV–Vis absorption spectra were obtained at room temperature by a Gold Spectrumlab 54 UV–Vis spectrophotometer. Fluorescence spectra were carried

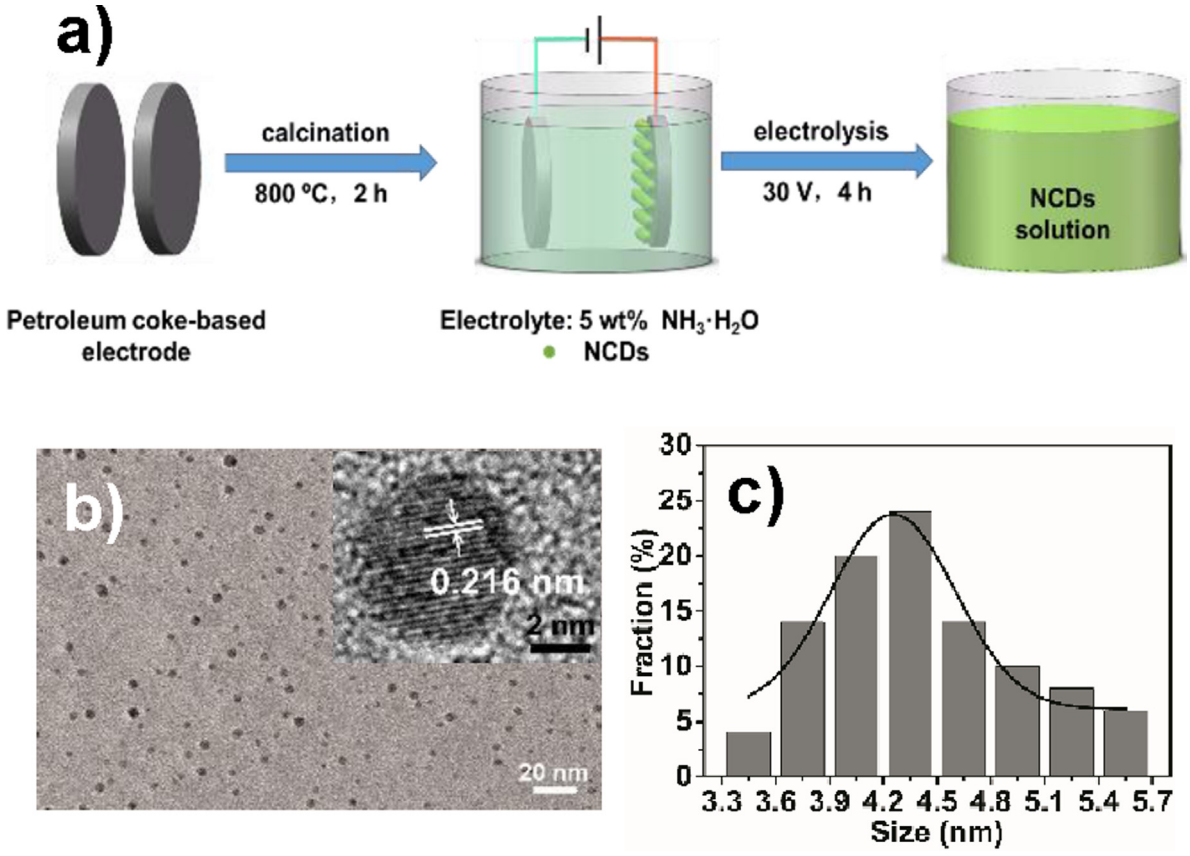

Fig. 1. a) Schematic illustration of the synthesis of petroleum coke-based NCDs. b) TEM and HRTEM images (inset) of NCDs. c) The size distribution of NCDs obtained from multiple images. (A colour version of this figure can be viewed online.)

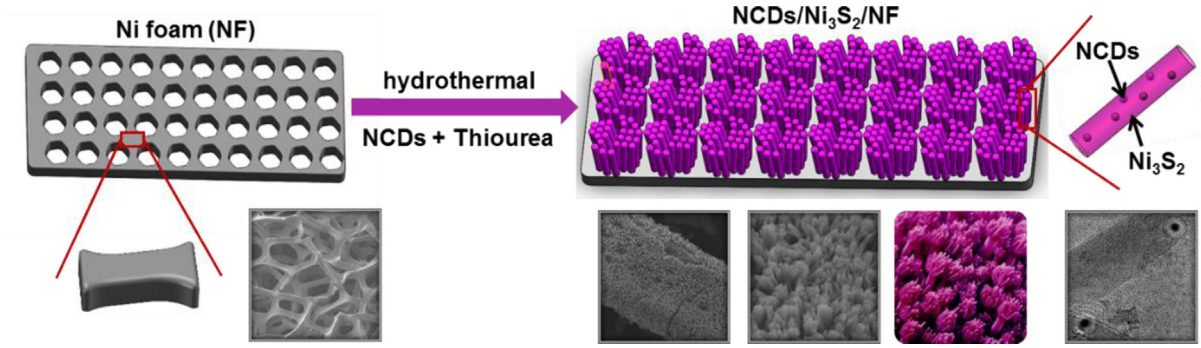

Fig. 2. Schematic illustration of the synthesis of coral-like NCDs/Ni_3S_2/NF electrode. (A colour version of this figure can be viewed online.)

out at room temperature on an F-97 Pro spectrofluorometer. The elemental measurement of C, H, and N were acquired on a Varo EL III elemental analyzer. Fourier transform infrared (FT-IR) spectra were measured at a Nicolet 6700 spectrometer. XPS measurements were conducted on an ESCALAB 250XI X-ray photoelectron spectrometer. SEM characterizations were performed on a ZEISS MERLIN scanning electron microscope at 20 kV. STEM characterizations were recorded by a JEM2100F scanning transmission electron microscopy (JEOL, Japan) at 200 kV. All self-standing electrodes were characterized by using the resultant materials directly.

2.5. Electrochemical measurements

All electrochemical measurements were conducted on a CHI 760E electrochemical workstation (CHI Instruments, Inc., Shanghai) with a standard three-electrode system, employing the resultant materials (0.8 cm × 0.8 cm) as the working electrode, a carbon rod as the counter electrode and an Ag/AgCl electrode as the reference electrode. All potentials reported were calibrated to reversible hydrogen electrode (RHE) according to E (RHE) = E (Ag/AgCl) + 0.197 V + 0.059 × pH [2]. The linear sweep voltammetry (LSV) curves were recorded in the range of 0 to −0.6 V versus RHE at a scan rate of 5 mV/s. The long-term durability of as-prepared materials was evaluated through chronoamperometric measurements. All voltammograms in this study were plotted without iR drop compensation. For comparison, benchmark materials (20 wt% Pt/C and RuO_2) loaded on NF as the working electrodes were prepared, with the same loading mass and working surface area of NCDs/Ni_3S_2/NF. In a typical procedure: (1) 6 mg 20 wt% Pt/C or RuO_2 powder and 10 μL 5 wt% Nafion solution were dispersed in 800 μL absolutely ethanol, then sonicated for 60 min to gain a homogeneous mixture, (2) 363 μL of this solution was drop-casted onto NF (0.8 cm × 0.8 cm) with the loading amount of 4.2 mg cm^{-2}, (3) 80 μL of 0.5 wt% Nafion solution in absolutely ethanol was pipetted onto the electrode to protect the catalyst, then left to dry in air. The electrochemically active surface area (ECSA) is proportional to the electrochemical double-layer capacitance (C_{dl}) value in the same material, which can be derived from the linear slope of the current density versus scan rate by collecting cyclic voltammograms (CV) in a non-Faradaic region [22]. To be specific, a series of CV measurements were conducted using a two-electrode electrolyzer at various scan rate of 10, 20, 40, 60, 80, 100 mV/s in the range of 0.1–0.2 V versus RHE. A linear slope can be calculated through plotting the current density between the anode and cathode ($j_{anodic} - j_{cathodic}$) at 0.15 V versus RHE against the scan rate.

3. Results and discussion

3.1. Morphology and structural information

The typical transmission electron microscopy (TEM) image (Fig. 1b) reveals the quasi-sphere morphology and monodispersity of the as-prepared NCDs, and no other salt particles or impurities were observed. The high-resolution TEM (HRTEM) image of NCDs particle (Fig. 1b, inset) shows the crystal lattice spacing of around 0.216 nm, which is consistent with the (100) lattice planes of graphitic carbon [23]. Through random statistics of 100 particles, the NCDs display a narrow diameter distribution with an average diameter of 4.42 ± 0.15 nm (Fig. 1c). The formation of NCDs is further confirmed by XRD (Fig. S1a), UV–vis and photoluminescence (PL) spectra (Fig. S2) and Raman spectra (Fig. S3). The Fourier-transform infrared (FT-IR) spectroscopy (Fig. S4) and X-ray photoelectron spectroscopy (XPS) (Fig. S5) reveal that the as-prepared NCDs contain various oxygen- and nitrogen-containing functional groups, especially with a quite high percentage of nitrogen (18.48 wt%, Table S1).

The digital photographs of NCDs/Ni_3S_2/NF before and after being stretched (Figs. S6a and S6b) indicate that this structure is flexible and capable of directly acting as an integrated electrode. The crystallographic structure and phase purity of resultant NCDs/Ni_3S_2/NF are given in Fig. 3a. The broader diffraction peak of NCDs around 26° ascribed to (002) plane of graphitic carbon is not quite obvious due to the interference of Ni_3S_2 and metallic Ni [24]. The formation of Ni_3S_2 (Fig. S7a) and the decorated NCDs (Fig. S7b) can be further confirmed by Raman spectroscopy. The XPS spectra in the Ni 2p, S 2p, C 1s, N 1s and O 1s regions are shown in Figs. S8–S10. The low-magnification scanning electron microscopy (SEM) images of NCDs/Ni_3S_2/NF in Fig. 3c display a coral-like morphology fully covering the surface of NF. The 3D macroporous structure (Fig. 3b) is consistent with the pristine NF (Fig. S11). The high-magnification SEM image (Fig. 3d) further reveals that the nanoclusters grow vertically on NF, and every nanocluster consists of several nanorods with diameter about 35 nm. The TEM image in Fig. 3e shows that the NCDs/Ni_3S_2 nanoclusters possess a smooth surface and the NCDs are fully embedded in Ni_3S_2 nanorods with a slight aggregation that the diameter of NCDs increase to ~6 nm (the black dots are NCDs which result in a decreased density of surrounding Ni_3S_2). In the HRTEM image taken from the NCDs/Ni_3S_2 nanorods (Fig. 3f), three sets of lattice fringes are observed, giving interplanar distance of 0.24 and 0.28 nm corresponding to the (003) and (110) crystallographic planes of hexagonal Ni_3S_2 phase [13,25], and the angle between the two facets is 55.4°, which

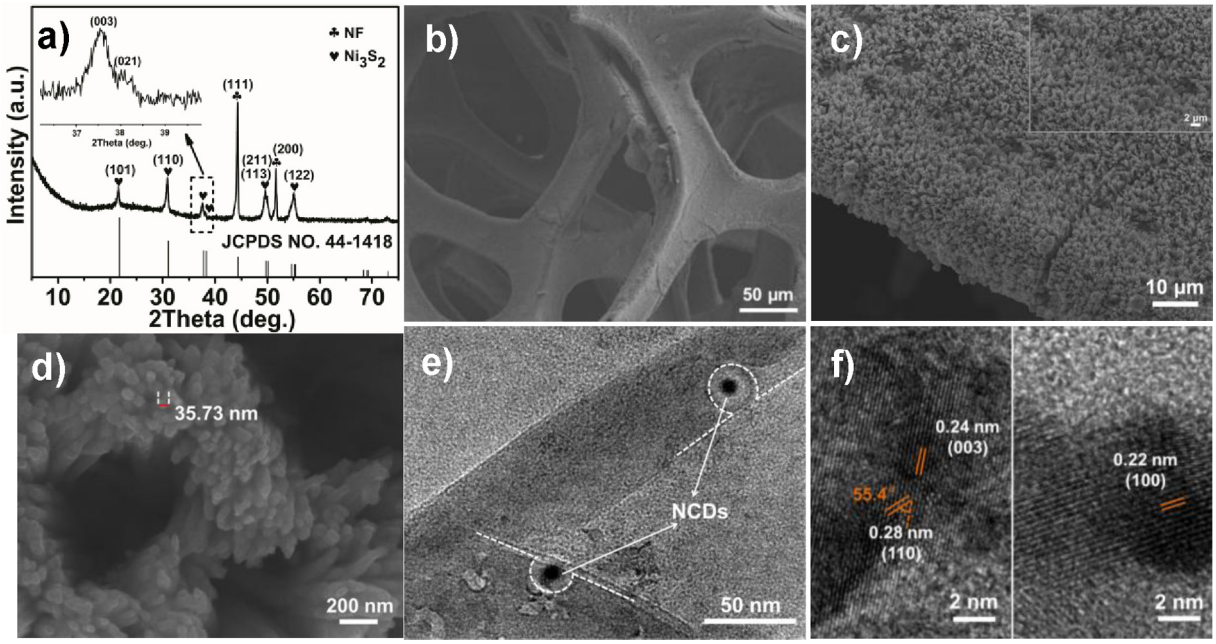

Fig. 3. a) XRD pattern of NCDs/Ni_3S_2/NF. b, c) Low- and d) high-magnification SEM images of NCDs/Ni_3S_2/NF. e) TEM and f) HRTEM images taken from NCDs/Ni_3S_2 nanoclusters. (A colour version of this figure can be viewed online.)

indicates that the exposed facet of the Ni_3S_2 nanoclusters is {021} high-index facet (Fig. S12). The lattice fringe with an interplanar spacing of 0.22 nm is in accordance with the (100) lattice planes of petroleum coke-based NCDs. Fig. S13 shows STEM image and the corresponding elemental mapping images of C, N, O, Ni and S demonstrate the uniform distribution of C, N, O, Ni and S elements in the NCDs/Ni_3S_2/NF electrode. Based on all above observations, a coral-like NCDs/Ni_3S_2/NF composite with NCDs/Ni_3S_2 nanoclusters uniformly distributed on the NF substrate is successfully prepared.

As a controllable experiment, pure water without NCDs was used in the hydrothermal treatment. The resultant NF was covered by irregular Ni_3S_2 nanosheets (Figs. S14 and S15), which is similar to previously report [13]. This suggests the NCDs play crucial roles during the synthesis of NCDs/Ni_3S_2/NF composites. To be specific, by comparing the XPS spectra of Ni 2p in Ni_3S_2/NF and NCDs/Ni_3S_2/NF (Fig. S16a), the NCDs cause a red shift of Ni 2p, which is attributed to the electron-donating behavior of NCDs [26]. Presumably, the electrostatic interaction between NCDs and Ni may promote the growth of Ni_3S_2 into coral-like nano arrays, which deserve further study in the future.

3.2. Activities of NCDs/Ni_3S_2/NF toward OER

The OER performance of NCDs/Ni_3S_2/NF was investigated in 1.0 M KOH electrolyte with a three-electrode system, in which the NCDs/Ni_3S_2/NF was used as self-supported electrode, employing a carbon rod as counter electrode and an Ag/AgCl electrode as reference electrode. For controllable experiments, similar measurements for bare NF, RuO_2 modified NF (RuO_2/NF) and Ni_3S_2/NF were also implemented. As shown in Fig. 4a, the NCDs/Ni_3S_2/NF electrode exhibits much higher catalytic activity toward OER than bare Ni foam, RuO_2/NF and Ni_3S_2/NF. NCDs/Ni_3S_2/NF requires an overpotential of only 340 mV to reach 200 mA cm^{-2}, which is 71 mV lower than that of RuO_2/NF. This performance is also superior to that of many noble-metal-free bifunctional electrocatalysts reported elsewhere (Table S2). The oxidation peaks around 1.4 V vs RHE are mainly ascribed to the oxidative transformation of Ni^{II} to Ni^{III} [27]. But it's noteworthy that the peak of NCDs/Ni_3S_2/NF exhibits extremely stronger current intensity than that of Ni_3S_2/NF, which may arise from the intrinsically electronegative behavior of NCDs, leading to additional electronic transfer steps under positive voltage. The OER kinetics was also estimated by corresponding Tafel plots (η versus log(j)) of these electrodes (Fig. 4b). The Tafel slope for NCDs/Ni_3S_2/NF is 67 mV dec^{-1}, which is smaller than that of bare Ni foam (170 mV dec^{-1}), RuO_2/NF (129 mV dec^{-1}) and Ni_3S_2/NF (136 mV dec^{-1}), indicating a more rapid OER rate for NCDs/Ni_3S_2/NF. The durability of NCDs/Ni_3S_2/NF was characterized by measuring polarization between 1.0 and 1.8 V for 5000 cycles (Fig. 4c), the material gives almost the same polarization curve before and after scanning. Furthermore, the long-term electrochemical stability of NCDs/Ni_3S_2/NF electrode was also probed in 1.0 M KOH (Fig. 4d). Even after a duration of 24 h, its composition almost remains unchanged, as revealed by XRD pattern (Fig. S17a) and XPS spectra (Figs. S8, S9c and S10c). NCDs/Ni_3S_2/NF can largely retain the coral-like morphology (Fig. S17b), but it undergoes noticeable morphology changes during the reaction, which can be attributed to the oxidation of Ni_3S_2 in OER process. In particular, after 5000 cycles of OER reaction, the intensity of the peak of metallic Ni (852.1 eV, Fig. S8b) [28] turns weaker and a blue shift to 852.9 eV appears, indicating that the surface of NCDs/Ni_3S_2/NF may have been partly oxidized.

3.3. Activities of NCDs/Ni_3S_2/NF toward HER

The HER performance of NCDs/Ni_3S_2/NF was investigated in 1.0 M KOH electrolyte with a similar three-electrode system to OER performance, in which the NCDs/Ni_3S_2/NF was used as self-supported electrode. For controllable experiments, similar measurements of bare Ni foam, 20 wt% Pt/C on Ni foam (Pt-C/NF) and Ni_3S_2/NF were also implemented. As shown in Fig. 5a, NCDs/Ni_3S_2/NF exhibits an excellent catalytic activity toward HER, with an overpotential of 187 mV to drive 20 mA cm^{-2}, which is 171 and 131 mV lower than that of bare Ni foam and Ni_3S_2/NF. Compared to

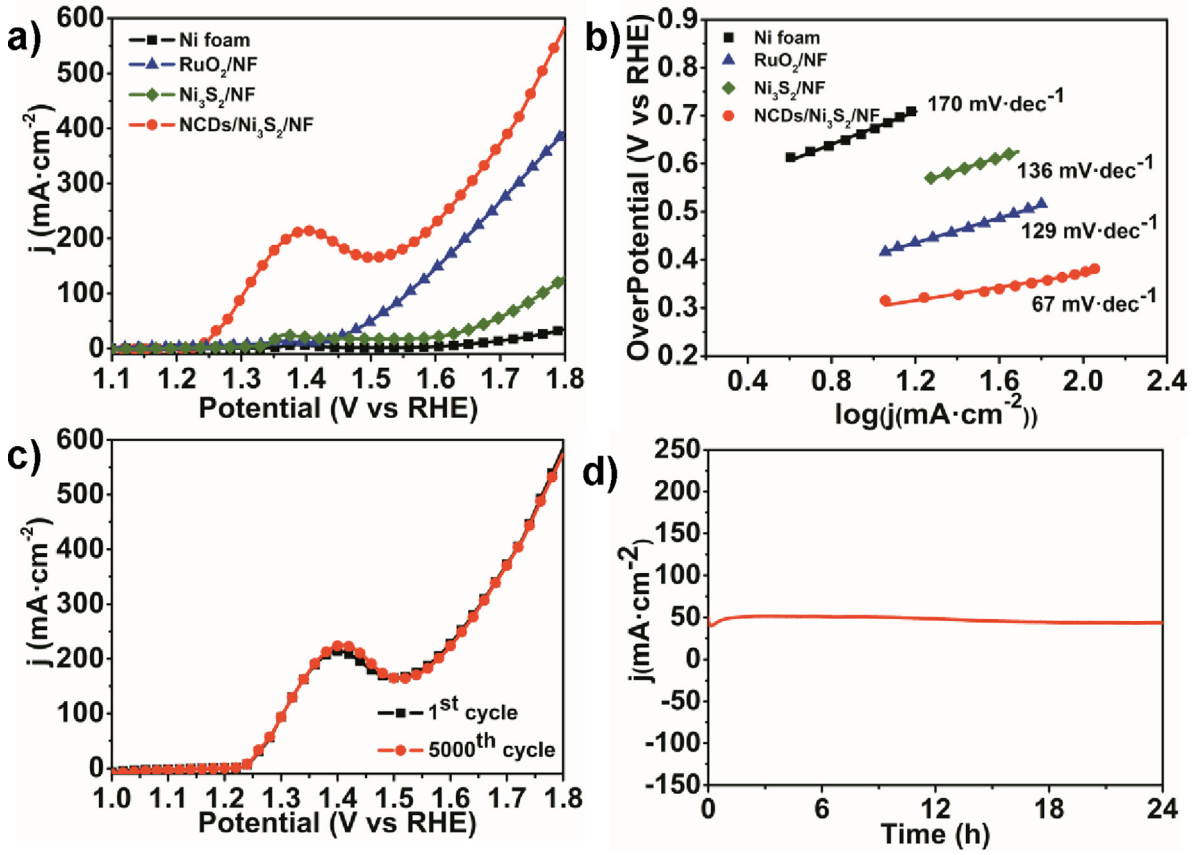

Fig. 4. a) LSV curves of NCDs/Ni_3S_2/NF, bare Ni foam, RuO_2/NF and Ni_3S_2/NF at a sweep rate of 5 mV/s without iR drop compensation. b) Tafel plots of NCDs/Ni_3S_2/NF, bare Ni foam, RuO_2/NF and Ni_3S_2/NF for OER. c) LSV curves for NCDs/Ni_3S_2/NF before and after potential sweeps between 1.0 and 1.8 V for 5000 cycles. d) Time-dependent current density curve of NCDs/Ni_3S_2/NF. (A colour version of this figure can be viewed online.)

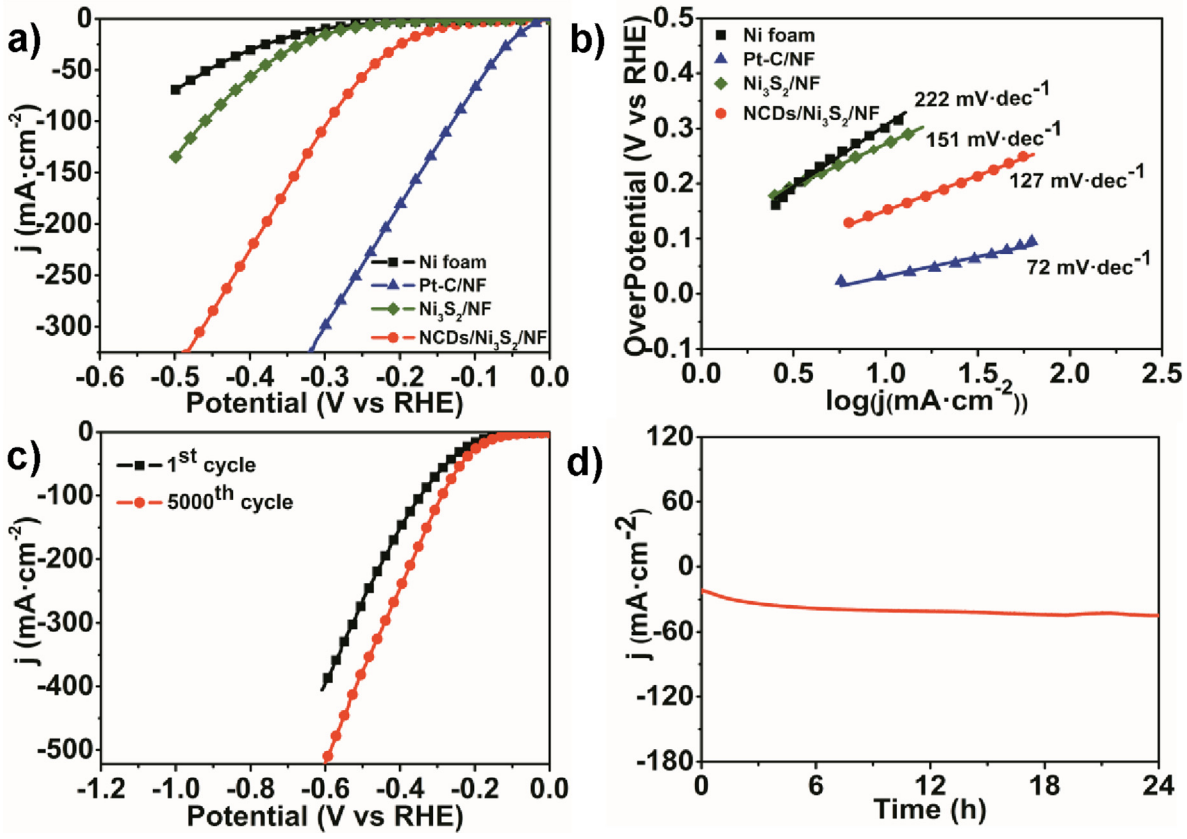

Fig. 5. a) LSV curves for NCDs/Ni_3S_2/NF, ba re Ni foam, Pt/C and Ni_3S_2/NF at a sweep rate of 5 mV/s without iR drop compensation. b) Tafel plots of NCDs/Ni_3S_2/NF, bare Ni foam, Pt/C and Ni_3S_2/NF for HER. c) LSV curves for NCDs/Ni_3S_2/NF before and after potential sweeps between 0 and -0.6 V for 5000 cycles. d) Time-dependent current density curve of NCDs/Ni_3S_2/NF at a static overpotential of 187 mV over 24 h. (A colour version of this figure can be viewed online.)

most reported noble-metal-free bifunctional electrocatalysts, NCDs/Ni_3S_2/NF exhibits a relatively lower overpotential (Table S2). The corresponding Tafel slopes of NCDs/Ni_3S_2/NF, bare Ni foam, Pt-C/NF and Ni_3S_2/NF are 127, 222, 72 and 151 mV dec^{-1}, respectively (Fig. 5b). The durability of NCDs/Ni_3S_2/NF was evaluated by measuring polarization between 0 and -0.6 V for 5000 cycles (Fig. 5c). During the long-term electrochemical stability testing at a static overpotential of 187 mV, NCDs/Ni_3S_2/NF also shows a higher current with excellent durability (Fig. 5d). These incremental phenomena may arise from the synergistic effect of NCDs/Ni_3S_2 nanoclusters and metallic Ni generated by cathodic reduction. More specifically, along with the multi-cycling of HER reaction, slight amount of high valence Ni over NCDs/Ni_3S_2 nanoclusters may be randomly reduced into metallic Ni as evident from the corresponding Ni 2p XPS spectra (Fig. S8b) where the intensity of the peak at 852.1 eV indexed to metallic Ni [28] turns stronger and a red shift appears after long-term HER testing, indicating the electrical conductivity and electron transfer rate of NCDs/Ni_3S_2/NF are improved. Furthermore, the unfilled d orbitals of high valence Ni in Ni_3S_2 have strong electrostatic attraction to OH^-, which markedly accelerate the key step of water electrolysis ($H_2O + e^- \rightarrow H_{ad} + OH^-$) [29]. Meanwhile, transition metals including Ni are good at adsorbing and recombining the reactive hydrogen intermediates (H_{ad}) [30]. Thus, the hydrogen production will be more efficient with numerous NCDs/Ni_3S_2-Ni system on NCDs/Ni_3S_2/NF. The morphology and microstructure of NCDs/Ni_3S_2/NF are nearly unchanged, neglecting the slight merge of nanorod edge, as evident from its XRD pattern (Fig. S18a), SEM image (Fig. S18b) and XPS spectra (Figs. S8, S9b and S10b). Additionally, the NCDs/Ni_3S_2/NF is also effective for HER in acidic media, which is completely different with previous report on Ni_3S_2/NF (Figs. S19–S21) [13], which suggests the NCDs/Ni_3S_2/NF have a potential for HER in the whole range of pH value.

3.4. Activities of NCDs/Ni_3S_2/NF toward overall water splitting

Given that NCDs/Ni_3S_2/NF exhibits remarkable bifunctional electrocatalytic property for OER and HER in 1.0 M KOH. An electrolyzer using NCDs/Ni_3S_2/NF as both anode and cathode was assembled for overall water splitting. The system affords a current density of 10 mA cm^{-2} at 1.50 V (Fig. 6a), which is only 20 mV higher than that of Pt-C/NF || RuO_2/NF. Surprisingly, NCDs/Ni_3S_2/NF even requires a smaller applied potential compared with Pt-C/NF || RuO_2/NF when the current density exceeds 80 mA cm^{-2}. Finally, the NCDs/Ni_3S_2/NF electrodes exhibit excellent stability for 24 h electrolytic reaction (Fig. 6b). Furthermore, the electrolyzer can be run with a single-cell AAA battery of 1.5 V (Fig. 6c), and large volumes of H_2 and O_2 gases generate on the cathode and anode respectively. The above results also indicate that the catalytic performance of NCDs/Ni_3S_2/NF is superior to those of most previously reported bifunctional electrocatalysts for overall water splitting (Table S2).

The excellent performance of NCDs/Ni_3S_2/NF for overall water splitting is attributed to the following reasons. (1) NCDs promote the growth of Ni_3S_2 to coral-like morphology with more {021} high-index facets exposed, which can provide more desirable surface atomic structures (such as more atomic steps [31,32]) for catalytic process than low-index faceted Ni_3S_2 [13]. (2) The coral-like architecture of NCDs/Ni_3S_2/NF provides large active areas and numerous accessible catalytic sites, which can be evident from the

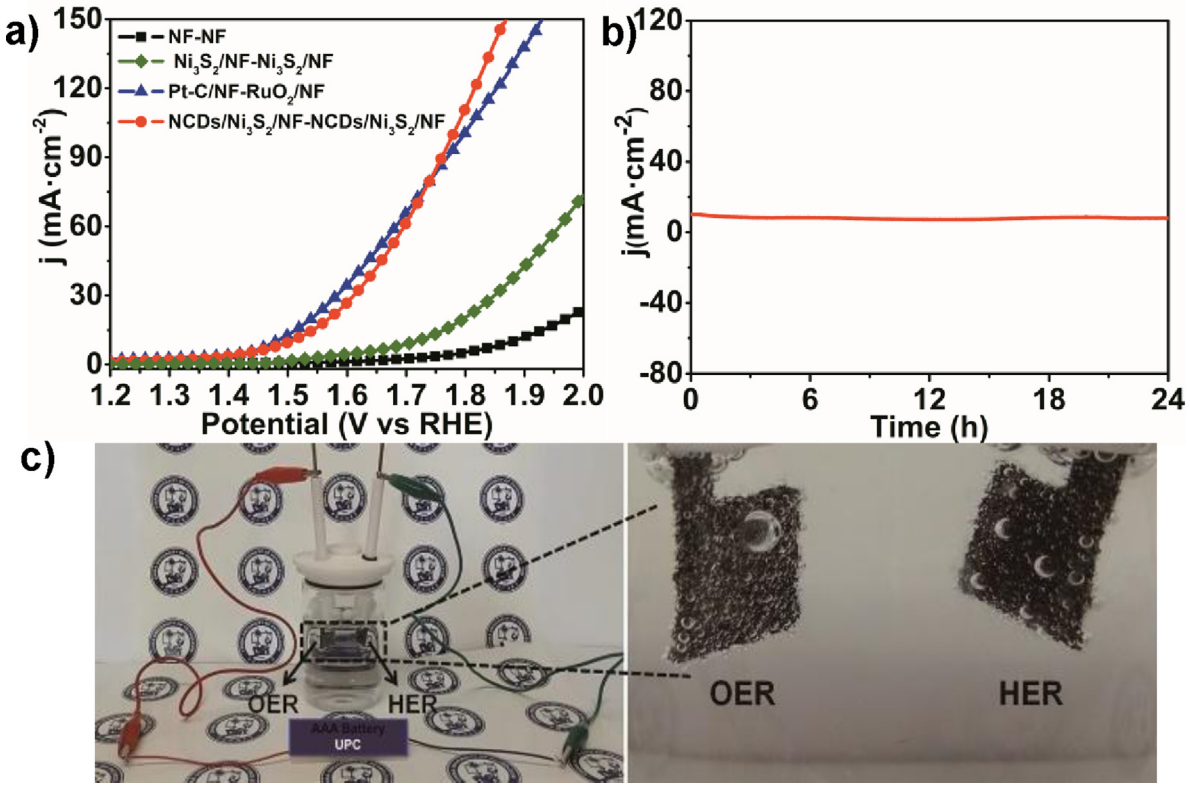

Fig. 6. a) Polarization curves of electrolyzers containing NCDs/Ni_3S_2/NF-NCDs/Ni_3S_2/NF, Ni_3S_2/NF-Ni_3S_2/NF, Ni foam-Ni foam or Pt/C-RuO_2 couple for overall water splitting at a scan rate of 5 mV/s without iR drop compensation. b) Chronoamperometric curve of water electrolysis for NCDs/Ni_3S_2/NF in a two-electrode configuration with constant current density of 10 mA cm^{-2} c) Photographs of an electrolyzer with NCDs/Ni_3S_2/NF as both anode and cathode, powered by a single-cell AAA battery of 1.5 V. (A colour version of this figure can be viewed online.)

fact that NCDs/Ni_3S_2/NF has more than 15 times higher electrochemical active area than Ni_3S_2/NF (Fig. S22). (3) The presence of NCDs embedded in Ni_3S_2 nanorods effectively increases the fast charge transfer pathways (Fig. S23) and protect NCDs/Ni_3S_2/NF from corrosion or agglomeration in alkaline and acidic solution, contributing to its prominent catalytic stability.

4. Conclusions

In summary, a novel one-step electrochemical approach has been developed for facile synthesis of NCDs from petroleum coke using ammonia solution as electrolyte, during which the tedious dialysis and purification steps are avoided. The NCDs can be well dispersed in water and promote the in-situ formation of well-defined coral-like NCDs/Ni_3S_2/NF composites by hydrothermal method. The coral-like NCDs/Ni_3S_2/NF composites can be directly used as both anode and cathode for water splitting, possessing superior catalytic activity and durability. This work marks a significant step toward the massive preparation of NCDs and the development of NCDs-modified non-noble electrocatalysts.

Acknowledgements

This work was financially supported by the National Natural Science Foundation of China (Nos. 51572296, U1662113, 51372277); the Fundamental Research Funds for the Central Universities of China (Nos. 15CX08005A, 14CX02127A); the Shandong Provincial Natural Science Foundation (ZR2016BB18); the Fundamental Research Fund for the Central Universities (No. 18CX02015A).

Appendix A. Supplementary data

Supplementary data related to this article can be found at https://doi.org/10.1016/j.carbon.2017.12.040.

References

[1] X.X. Zou, Y. Zhang, Noble metal-free hydrogen evolution catalysts for water splitting, Chem. Soc. Rev. 44 (2015) 5148–5180.
[2] M. Ledendecker, S. Krick Calderon, C. Papp, H.P. Steinruck, M. Antonietti, M. Shalom, The synthesis of nanostructured Ni_5P_4 films and their use as a non-noble bifunctional electrocatalyst for full water splitting, Angew. Chem. Int. Ed. 54 (2015) 12361–12365.
[3] N.T. Suen, S.F. Hung, Q. Quan, N. Zhang, Y.J. Xu, H.M. Chen, Electrocatalysis for the oxygen evolution reaction: recent development and future perspectives, Chem. Soc. Rev. 46 (2017) 337–365.
[4] J.Q. Tian, Q. Liu, A.M. Asiri, X.P. Sun, Self-supported nanoporous cobalt phosphide nanowire arrays: an efficient 3D hydrogen-evolving cathode over the wide range of pH 0-14, J. Am. Chem. Soc. 136 (2014) 7587–7590.
[5] S. Zhang, X.B. Yu, F. Yan, C.Y. Li, X.T. Zhang, Y.J. Chen, N-Doped graphene-supported Co@CoO core–shell nanoparticles as high-performance bifunctional electrocatalysts for overall water splitting, J. Mater. Chem. 4 (2016) 12046–12053.
[6] Z.H. Yin, Y. Sun, C.L. Zhu, C.Y. Li, X.T. Zhang, Y.J. Chen, Bimetallic Ni–Mo nitride nanotubes as highly active and stable bifunctional electrocatalysts for full water splitting, J. Mater. Chem. 5 (2017) 13648–13658.
[7] Z.X. Yin, S. Zhang, Y.J. Chen, P. Gao, C.L. Zhu, P.P. Yang, et al., Hierarchical nanosheet-based $NiMoO_4$ nanotubes: synthesis and high supercapacitor performance, J. Mater. Chem. 3 (2015) 739–745.
[8] S.K. Wu, X.P. Shen, G.X. Zhu, E. Zhou, Z.Y. Ji, L.B. Ma, et al., Metal organic framework derived NiFe@N-doped graphene microtube composites for hydrogen evolution catalyst, Carbon 116 (2017) 68–76.
[9] F. Yan, C.L. Zhu, C.Y. Li, S. Zhang, X.Y. Zhang, Y.J. Chen, Highly stable three-dimensional nickel–iron oxyhydroxide catalysts for oxygen evolution reaction at high current densities, Electrochim. Acta 245 (2017) 770–779.
[10] F. Yan, Y. Wang, K.Y. Li, C.L. Zhu, P. Gao, C.Y. Li, et al., Highly stable three-dimensional porous nickel-iron nitride nanosheets for full water splitting at high current densities, Chem. Eur J. 23 (2017) 10187–10194.
[11] X.B. Yu, S. Zhang, C.Y. Li, C.L. Zhu, Y.J. Chen, P. Gao, et al., Hollow CoP nanoparticle/N-doped graphene hybrids as highly active and stable bifunctional catalysts for full water splitting, Nanoscale 8 (2016) 10902–10907.
[12] Z.X. Yin, C.L. Zhu, C.Y. Li, S. Zhang, X.T. Zhang, Y.J. Chen, Hierarchical nickel–cobalt phosphide yolk–shell spheres as highly active and stable bifunctional electrocatalysts for overall water splitting, Nanoscale 35 (2016) 19129–19138.
[13] X.Y. Liu, X. Wang, X.T. Yuan, W.J. Dong, F.Q. Huang, Rational composition and structural design of in situ grown nickel-based electrocatalysts for efficient water electrolysis, J. Mater. Chem. 4 (2016) 167–172.
[14] D.Y. Chung, J.W. Han, D.H. Lim, J.H. Jo, S.J. Yoo, H. Lee, et al., Structure dependent active sites of Ni_xS_y as electrocatalysts for hydrogen evolution reaction, Nanoscale 7 (2015) 5157–5163.
[15] J. Liu, Y. Liu, N.Y. Liu, Y.Z. Han, X. Zhang, H. Huang, et al., Metal-free efficient photocatalyst for stable visible water splitting via a two-electron pathway, Science 347 (2015) 970–974.
[16] W.J. Zhou, X.J. Wu, X.H. Cao, X. Huang, C.L. Tan, J. Tian, et al., Ni_3S_2 nanorods/Ni foam composite electrode with low overpotential for electrocatalytic oxygen evolution, Energy Environ. Sci. 6 (2013) 2921–2924.
[17] Y.M. Yang, J. Liu, S.J. Guo, Y. Liu, Z.H. Kang, A nickel nanoparticle/carbon quantum dot hybrid as an efficient electrocatalyst for hydrogen evolution under alkaline conditions, J. Mater. Chem. 3 (2015) 18598–18604.
[18] K.A. Fernando, S. Sahu, Y.M. Liu, W.K. Lewis, E.A. Guliants, A. Jafariyan, et al., Carbon quantum dots and applications in photocatalytic energy conversion, ACS Appl. Mater. Interfaces 7 (2015) 8363–8376.
[19] X.D. Shao, W.T. Wu, R.Q. Wang, J.Q. Zhang, Z.T. Li, Y. Wang, et al., Engineering surface structure of petroleum-coke-derived carbon dots to enhance electron transfer for photooxidation, J. Catal. 344 (2016) 236–241.
[20] W.T. Wu, L.Y. Zhan, W.Y. Fan, J.Z. Song, X.M. Li, Z.T. Li, et al., Cu-N dopants boost electron transfer and photooxidation reactions of carbon dots, Angew. Chem. Int. Ed. 54 (2015) 6540–6544.
[21] J.J. Lv, J. Zhao, H. Fang, L.P. Jiang, L.L. Li, J. Ma, et al., Incorporating nitrogen-doped graphene quantum dots and Ni_3S_2 nanosheets: a synergistic electrocatalyst with highly enhanced activity for overall water splitting, Small 24 (2017), 1700264.
[22] T. Yoon, K.S. Kim, One-step synthesis of CoS-doped β-$Co(OH)_2$@amorphous MoS_{2+x} hybrid catalyst grown on nickel foam for high-performance electrochemical overall water splitting, Adv. Funct. Mater. 26 (2016) 7386–7393.
[23] H. Huang, H.L. Hu, S. Qiao, L. Bai, M.M. Han, Y. Liu, et al., Carbon quantum dot/CuS_x nanocomposites towards highly efficient lubrication and metal wear repair, Nanoscale 7 (2015) 11321–11327.
[24] M.B. Wu, Y. Wang, W.T. Wu, C. Hu, X.N. Wang, J.T. Zheng, et al., Preparation of functionalized water-soluble photoluminescent carbon quantum dots from petroleum coke, Carbon 78 (2014) 480–489.
[25] L.L. Feng, G.T. Yu, Y.Y. Wu, G.D. Li, H. Li, Y.H. Sun, et al., High-index faceted Ni_3S_2 nanosheet arrays as highly active and ultrastable electrocatalysts for water splitting, J. Am. Chem. Soc. 137 (2015) 14023–14026.
[26] X.M. Li, M.C. Rui, J.Z. Song, Z.H. Shen, H.B. Zeng, Carbon and graphene quantum dots for optoelectronic and energy devices: a review, Adv. Funct. Mater. 25 (2015) 4929–4947.
[27] C. Tang, N.Y. Cheng, Z.H. Pu, W. Xing, X.P. Sun, NiSe nanowire film supported on nickel foam: an efficient and stable 3D bifunctional electrode for full water splitting, Angew. Chem. Int. Ed. 54 (2015) 9351–9355.
[28] X. Li, G.Q. Han, Y.R. Liu, B. Dong, W.H. Hu, X. Shang, et al., NiSe@NiOOH core-shell hyacinth-like nanostructures on nickel foam synthesized by in situ electrochemical oxidation as an efficient electrocatalyst for the oxygen evolution reaction, ACS Appl. Mater. Interfaces 8 (2016) 20057–20066.
[29] Y. Rao, Y. Wang, H. Ning, P. Li, M.B. Wu, Hydrotalcite-like Ni(OH)(2) nanosheets in situ grown on nickel foam for overall water splitting, ACS Appl. Mater. Interfaces 8 (2016) 33601–33607.
[30] L. Wang, C. Lin, D.K. Huang, J.M. Chen, L. Jiang, M.K. Wang, et al., Optimizing the volmer step by single-layer nickel hydroxide nanosheets in hydrogen evolution reaction of platinum, ACS Catal. 5 (2015) 3801–3806.
[31] C. Chen, Y.J. Kang, Z.Y. Huo, Z.W. Zhu, W.Y. Huang, H.L. Xin, et al., Highly crystalline multimetallic nanoframes with three-dimensional electrocatalytic surfaces, Science 343 (2014) 1339–1343.
[32] Y.J. Kang, P.D. Yang, N.M. Markovic, V.R. Stamenkovic, Shaping electrocatalysis through tailored nanomaterials, Nano Today 11 (2016) 587–600.